# Bayesian Model for Multisensory Integration and Segregation

by

Xiangyu Ma

A PhD Qualifying Report Submitted to
The Hong Kong University of Science and Technology
in Partial Fulfillment of the Requirements for
the Degree of Doctor of Philosophy
in Physics Graduate Program

June 2019, Hong Kong

# Authorization

I hereby declare that I am the sole author of the thesis.

I authorize the Hong Kong University of Science and Technology to lend this report to other institutions or individuals for the purpose of scholarly research.

I further authorize the Hong Kong University of Science and Technology to reproduce the report by photocopying or by other means, in total or in part, at the request of other institutions or individuals for the purpose of scholarly research.

---

Xiangyu Ma

June 2019

# Bayesian Model for Multisensory Integration and Segregation

by

Xiangyu Ma

This is to certify that I have examined the above PhD Qualifying Report
and have found that it is complete and satisfactory in all respects,
and that any and all revisions required by
the PhD Qualifying Examination Committee have been made.

---

Prof. K. Y. Michael Wong, Thesis Supervisor

---

Prof. Michael S. Altman, Head of Department

Department of Physics, HKUST

June 2019

# Acknowledgments

Foremost, I would like to thank my supervisor, Prof. Michael Wong, for the continuous support of my Ph.D study and research, for his patience and kindness. His guidance helped me doing research and writing a thesis.

Besides my advisor, I would like to thank the rest of my thesis committee: Prof. Michael Wong, Prof. Yilong Wang, and Prof. Jingdi Zhang, for their encouragement, insightful comments, and hard questions.

My sincere thanks also goes to current and former group members: Dr. Wenhao Zhang, Dr. He Wang, and Dr. Min Yan, leading me working on this exciting project.

Last but not the least, I would like to thank my parents.

# Contents

Title Page i

Authorization Page ii

Signature Page iii

Acknowledgments iv

Table of Contents v

List of Figures vii

Abstract ix

1 Introduction 1

1.1 Background of Multisensory Studies 1

1.2 Near Optimal Model for Multisensory Integration and Segregation 1

1.3 Motivation of This Work 4

1.4 Outline of This Report 4

2 Basic Functions for Circular Variables 5

2.1 Von Mises Basic Functions 5

2.2 Recursive Relation 6

2.3 Convolution 8

2.4 Approximation 8

3 Projection Methods for Network Dynamics 12

3.1 Bump Position 12

3.2 Noise Variance 13

4 Bayesian Inference 16
4.1 Incompleteness of Old Model 16
4.2 Output-Dependent Noise 17
4.3 Results of Modified Noise Variance 19

5 Priors with an Independent Component 22
5.1 Network Model 22
5.2 Vector Space 24
5.3 Information Segregation 25

6 Conclusion 27
6.1 Bayesian Model 27
6.2 Causal Inference 28

Reference 29

# List of Figures

1.1 Decentralized module. MSTd and VIP refer to different modules, which consist of two groups of neurons, congruent (blue circles) and opposite (red circle) neurons. Neurons are all connected to the inhibitory pool in each module, which receives the feedforward input respectively (up arrow). Adapted from Ref. [1]. 2

2.1 Illustration of the approximation and Fourier basis. A: the ratio of estimated value to actual value for previous approximation (first row) and modified approximation (second row) given two concentration ($\kappa_1,\ \kappa_2$) and angular disparity ($\theta$), color indicates the magnitude of the ratio. B: Function $I_x(a)/I_0(a)$ for different width $a$. 9

3.1 Bump profiles (synaptic inputs) of congruent and opposite groups in module 1 without noise. The blue and red colors represent congruent and opposite groups respectively. Solid lines: simulation results, dashed lines: analytic results by using projection method. 14

4.1 Weak input ($I_1 = I_2 = 0.01U_0$, left column) and strong input ($I_1 = I_2 = 0.7U_0$, right column). Symbols: network results; dashed lines: Bayesian prediction. The blue and red colors represent congruent and opposite groups in module 1 respectively. 19

5.1 Outputs from second layer with varying probability $p_0$. Illustration of the population response of congruent and opposite groups in module 1 applying weak inputs (A) and strong inputs (B). Symbols: network results; dashed lines: Bayesian prediction. The blue and red colors represent congruent and opposite groups in module 1 respectively. 23

5.2 Geometric interpretation of vector space. Colored vectors represent the sum of other vectors (black). Outputs from first layer: $\kappa_{1c}$ (congruent) and $\kappa_{1o}$ (opposite), second layer: $\kappa'_{1c}$ (congruent) and $\kappa'_{1o}$ (opposite). Note that the vectors (black) have been rescaled by $p_0$ and $1 - p_0$. 25

5.3 Outputs from second layer with varying input strength. From left to right, $I = 0.01U_0,\ 0.05U_0,\ 0.09U_0$. Colormap: color indicates the disparity $\Delta x$ of two cues. 26

6.1 Illustration of decentralized model after modification. New modules in the second layer. No connection between two groups of neurons in each module. The inputs and feedforward inputs from the first layer are rescaled by $1-p_0$ and $p_0$ respectively. Each group of neurons has their own inhibition pool and there's no reciprocal coupling between two modules. 28

# Bayesian Model for Multisensory Integration and Segregation

by Xiangyu Ma

Department of Physics, HKUST

The Hong Kong University of Science and Technology

Abstract

Multisensory integration and segregation are important for the survivorship of animals. The experimental data indicate that the brain processes information in an optimal way. On the other hand, an ideal model, which provided by Bayes rule to update the belief of the external world, is part of the fundamental bases of our future studies. The model suggested by Zhang et al. has demonstrated two different neuron groups are related to the multisensory integration and segregation simultaneously. However, his model is near optimal but lacking a theoretical understanding of the dynamics. In this report, we developed a novel method for revealing the dynamics behind this neural network and discuss the conditions for our new model to achieve Bayesian inference. Furthermore, we also suggest that an output-dependence noise and a new independent prior are necessary for the whole story.

# Chapter 1

# Introduction

## 1.1 Background of Multisensory Studies

Our brains process information from different sensory modalities. If two cues are received from the same source, the neural system will integrate these sensory signals. Otherwise, they should be segregated. For instance, when you are walking along a street, the signals originating in the visual and auditory stimuli will integrate together or segregate apart to improve the accuracy of perceptions of the moving objects. Theoretical insights, which have been derived from recent experimental techniques, reveal that some modalities could carry out specific tasks with the unique properties of neurons[2]. The whole story starts with the sensory perception, when external stimuli are given, the information received from multiple sensory organs will be decoded by evoked neural activities.

However, diverse modalities are able to provide the neural system with complementary information. Experimental data show that in the dorsal medial superior temporal (MSTd) area and the ventral intraparietal (VIP) area, there exist two types of neurons, congruent and opposite cells [3]. Here, we consider a recently proposed model in which the congruent and opposite neurons play a role in multisensory integration and segregation respectively [1]. In the following section, I will give a brief introduction of near optimal model in [1].

## 1.2 Near Optimal Model for Multisensory Integration and Segregation

We consider a neural network model [1] receiving external inputs of modality 1 and 2 with $I_m^{ext}(y,t),\ m = 1,2$, where $y$ is an angular variable in the range $(-\pi, \pi]$ and $t$ is

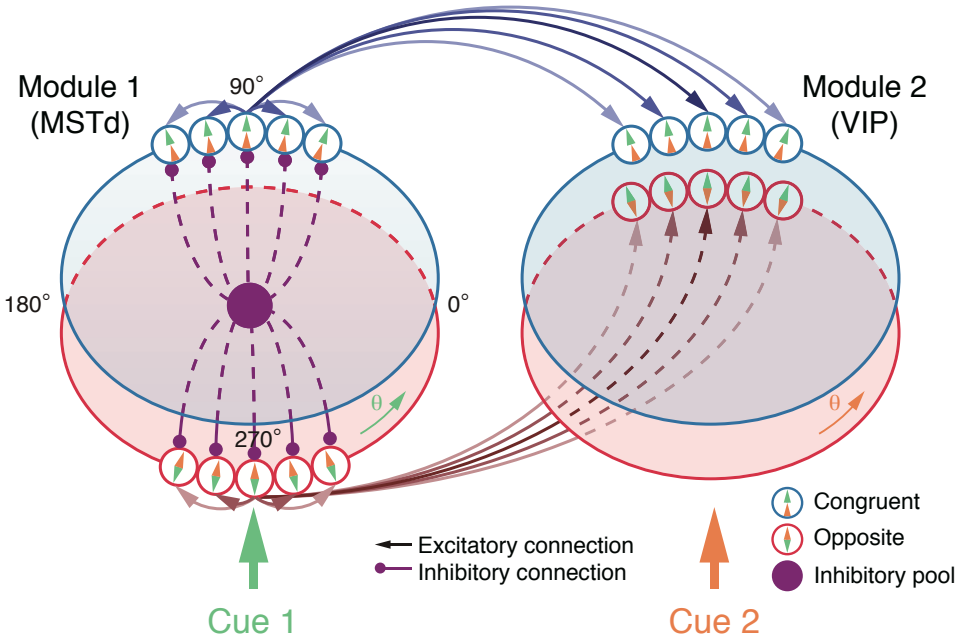


Figure 1.1: Decentralized module. MSTd and VIP refer to different modules, which consist of two groups of neurons, congruent (blue circles) and opposite (red circle) neurons. Neurons are all connected to the inhibitory pool in each module, which receives the feedforward input respectively (up arrow). Adapted from Ref. [1].

time. The two inputs are fed into two separate modules. Each module has two groups of congruent and opposite neurons, each neuron having a preferred stimulus $y$. The recurrent connections within each group are excitatory and dependent on the preferred stimuli of the neurons through a bump-shaped function of the separation of the stimulus positions, and there are global inhibitory connections connecting both groups, thus forming a continuous attractor neural network [4]. The congruent groups of each module are connected in a congruent manner, that is, neurons receiving inputs at position $x$ of each module are reciprocally connected to each other. Likewise, the opposite groups of each module are connected in an opposite manner, that is, neurons receiving inputs at position $x$ of one module are reciprocally connected to those at position $x + \pi$. Let $\psi_m(x,t)$ and $\bar{\psi}_m(x,t)$ be the synaptic input at position $x$ and time $t$ for the congruent and opposite groups respectively in module $m$, and denote as $\bar{m}$ the other module of module $m$. Then the

neuronal dynamics of the congruent group is given by

$$\tau\frac{\partial\psi_m(y,t)}{\partial t} = -\psi_m(y,t) + \sum_{y'=-\pi}^{\pi} J_{rc}V(y-y',a_0)R_m(y',t) + \sum_{y'=-\pi}^{\pi} J_{rp}V(y-y',a_0)R_{\bar{m}}(y',t) + I_m^{ext}(y,t), \tag{1.1}$$

where $J_{rc}$ and $J_{rp}$ represent the strengths of the recurrent and reciprocal couplings respectively. $R_m(y,t)$ is the firing rate of the neurons at position $y$ and $t$. It is given by $R_m(y,t) \equiv \psi_m^2(y,t)/D_m$, where $D_m \equiv 1+\omega\left[\sum_y \psi_m^2(y,t) + J_{int}\sum_y \bar{\psi}_m^2(y,t)\right]$ is the global inhibition acting on the congruent group in module $m$. $V(y-y',a_0)$ is the von Mises function given by

$$V(y-y',a_0) \equiv \frac{\exp[a_0\cos(y-y')]}{2\pi I_0(a_0)}, \tag{1.2}$$

where $a_0$ is referred to as the concentration of the von Mises function, and $I_0(a_0)$ is the modified Bessel function of order 0 introduced to normalize the von Mises function.

In Eq. (1.1), we assign the external inputs to be the sum of a bump with constant background, plus its noisy component characterized by the Fano factor $F_0$,

$$I_m^{ext}(y,t) = I_m V(y-x_m,\frac{a_0}{2}) + I_b + \sqrt{F_0\hat{A}}\epsilon_m(y,t) \tag{1.3}$$

where $\epsilon_m(y,t)$ is white noise of zero mean and variance satisfying $\langle\epsilon_m(y,t),\epsilon_{m'}(y',t')\rangle = \delta_{mm'}\delta(y-y')\delta(t-t')$.

On the other hand, the neuronal dynamics of the opposite group is given by

$$\tau\frac{\partial\bar{\psi}_m(y,t)}{\partial t} = -\bar{\psi}_m(y,t) + \sum_{y'=-\pi}^{\pi} J_{rc}V(y-y',a_0)\bar{R}_m(y',t) + \sum_{y'=-\pi}^{\pi} J_{rp}V(y-y'+\pi,a_0)\bar{R}_{\bar{m}}(y',t) + I_m^{ext}(y,t). \tag{1.4}$$

These equations can be solved by numerical simulations to obtain the means and variances of the firing rates. In the framework of probabilistic population coding [5], the posterior estimates of the external inputs can be derived from these quantities. Using the projection method [4], we first attempted first order perturbation using the von Mises function and its derivative as the basis. They represent distortions of the height and position of the bump-shaped firing rate distributions respectively, but the calculated means and variances of the distributions deviated from the numerical results. A careful inspection of the firing rate distributions showed that their profiles were not calculated accurately. Hence, higher order perturbations describing the distortions in the height,

position, width and skewness have to be introduced. We approximate the solution to the dynamical equations to be

$$\begin{aligned}\psi_m =& u_{m0} + u_{m1}\cos(y_1 - s_1) + u_{m2}\cos 2(y_1 - s_1) \\ &+ u_{m3}\sin 2(y_1 - s_1),\ m = 1, 2.\end{aligned} \tag{1.5}$$

The background, height, position, width and skewness are largely determined by the coefficients $u_{m0},\ u_{m1},\ s_m,\ u_{m2}$ and $u_{m3}$ respectively. Multiplying both sides of Eqs. (1.1) and (1.4) by $1,\ \cos(y-s_m),\ \cos 2(y-s_m)$ and $\sin 2(y-s_m)$ in turn and integrating over $y$, we obtain the steady state equations for this set of coefficients after averaging over noise. By considering the linear perturbation around the steady state, the variance $\hat{\sigma}_m^2$ of the peak positions $\hat{s}_m$ can be found.

## 1.3 Motivation of This Work

Previous work by Zhang et al. is impressive, however, we want to formulate an ideal model for multisensory integration and segregation as a mathematical problem. Results in [1] are not quite satisfactory. Simulation reveals that our current model is near optimal while lacking theoretical insights.

On the one hand, a theoretical understanding is needed for our future exploration. On the other hand, our current model is dealing with the prior distribution which is fully correlated. An independent prior is necessary especially for causal inference.

## 1.4 Outline of This Report

Our report begins with a background introduction to our recent work of multisensory integration and segregation problem. In Chapter 2, I will derive a set of basic functions for circular variables. In chapter 3, I will introduce the projection methods to analyze the dynamics of our current model. In chapter 4, I will discuss the conditions of this model for achieving Bayesian inference. In chapter 5, I will add an independent component in the prior for causal inference. In chapter 6, I will conclude this report and discuss future directions based on current results.

# Chapter 2

# Basic Functions for Circular Variables

## 2.1 Von Mises Basic Functions

Basic functions are given in [4, 6] are eigenstates of quantum harmonic oscillators. Each function corresponds to a definite mode of the neural dynamics. However, those basic functions are Gaussians which are not convenient to apply to circular variables. In this chapter, we develop a new set of basic function of which the profile base on von Mises functions.

Firstly we give the definition of the integration $N_n(k)$

$$N_n(k) = \int_{-\pi}^{\pi} e^{k\cos\theta} \sin^n \theta d\theta. \tag{2.1}$$

Note that our basic functions are defined on $[-\pi, \pi)$ with a periodic boundary condition, $k$ refers to the concentration of the von Mises function. We can integrate by parts and then obtain the iterative expression of $N_n(k)$

$$\begin{aligned} N_n(k) &= \int_{-\pi}^{\pi} e^{k\cos\theta} \sin^n \theta d\theta \\ &= \frac{n-1}{k} \int_{-\pi}^{\pi} e^{k\cos\theta} \sin^{n-2}\theta \cos\theta d\theta \\ &= \frac{n-1}{k^2} \int_{-\pi}^{\pi} e^{k\cos\theta} \left[(n-3)\sin^{n-4}\theta\cos^2\theta - \sin^{n-2}\theta\right] d\theta \\ &= \frac{(n-1)(n-3)}{k^2} N_{n-4}(k) - \frac{(n-1)(n-2)}{k^2} N_{n-2}(k). \end{aligned} \tag{2.2}$$

The first few terms are given below

$$
\begin{aligned}
N_0(k) &= 2\pi I_0(k) \\
N_2(k) &= \frac{2\pi I_1(k)}{k} \\
N_4(k) &= \frac{6\pi}{k^2}\left[I_0(k) - \frac{2I_1(k)}{k}\right] \\
N_6(k) &= \frac{30\pi}{k^3}\left[-\frac{4}{k}I_0(k) + (1+\frac{8}{k^2})I_1(k)\right],
\end{aligned} \tag{2.3}
$$

where $I_0(k)$ and $I_1(k)$ are the modified Bessel function of order 0 and 1 respectively. $N_n'(k)$ denotes the derivative of $N_n(k)$ with respect to $k$.

## 2.2 Recursive Relation

We define $u_0 \equiv C_0 e^{k\cos\theta}$ as the zeroth order normalized basic function, where $C_N,\ N = 0, 1, 2, ...$ is a normalization factor. We notice the inner production

$$\langle u_0, u_0 \sin\theta\rangle = 0. \tag{2.4}$$

Therefore, we obtain the first order basic function $u_1 \equiv C_1 u_0 \sin\theta$. Furthermore, we can define the second order basic function

$$u_2 \equiv C_2(u_1 \sin\theta - u_0\langle u_0, u_1 \sin\theta\rangle). \tag{2.5}$$

Since $u_2$ is an even function, $u_2$ is orthogonal to $u_1$. We can prove $\langle u_2, u_0\rangle = 0$.

Suppose we have a set of basic functions satisfying the following conditions

$$\langle u_i, u_j\rangle = \delta_{i,j} \tag{2.6}$$

$$\langle u_i, u_j \sin\theta\rangle = r_{j-1}\delta_{i,j-1} + r_j\delta_{i,j+1}, \tag{2.7}$$

where $\delta$ is the Kronecker delta, $i, j = 0, 1, 2, ..., N-1$. We define $r_i \equiv \langle u_i, u_{i+1}\sin\theta\rangle$ and $u_n$ is given by

$$u_n \equiv C_N(u_{N-1}\sin\theta - u_{N-2}\langle u_{N-2}, u_{N-1}\sin\theta\rangle). \tag{2.8}$$

When $i < N$, we can prove

$$
\begin{aligned}
\langle u_i, u_N\rangle &= C_N\left[\langle u_i, u_{N-1}\sin\theta\rangle - \langle u_i, u_{N-2}\rangle < u_{N-2}, u_{N-1}\sin\theta\rangle\right] \\
&= C_N\left[r_{N-2}\delta_{i,N-2} + r_{N-2}\delta_{i,N} - r_{N-2}\delta_{i,N-2}\right] \\
&= 0.
\end{aligned} \tag{2.9}
$$

Furthermore, this recursive relation can be useful

$$u_i \sin\theta = r_{i-1}u_{i-1} + r_i u_{i+1}. \tag{2.10}$$

Similar to the proof of the completeness of Fourier expansion, the completeness of this set of basic function is easy to prove. We can construct a delta function $h(\theta)$ in this way

$$h(\theta) = C_k e^{k_0(\cos\theta - 1)}(1 - \sin^2\theta)^k, \ when\ k \to \infty, \tag{2.11}$$

where $C_k$ is chosen to make sure $\int_{-\pi}^{\pi} h(\theta)d\theta = 1$. Note that the delta function $h(\theta)$ is a linear combination of $e^{k_0\cos\theta}\sin^n\theta$, and $e^{k_0\cos\theta}\sin^n\theta$ could be written by a linear combination of our basic functions.

The first few terms of our basic functions are derived below

$$\begin{aligned}
u_0 &= c_0 e^{k\cos\theta} \\
u_1 &= c_1 e^{k\cos\theta}\sin\theta \\
u_2 &= c_2 e^{k\cos\theta}\left[\sin^2\theta - \frac{N_2(2k)}{N_0(2k)}\right] \\
u_3 &= c_3 e^{k\cos\theta}\left[\sin^3\theta - \frac{N_4(2k)}{N_2(2k)}\sin\theta\right].
\end{aligned} \tag{2.12}$$

The coefficients $c_i$ $i = 0, 1, 2, ...$ are listed

$$\begin{aligned}
c_0 &= \frac{1}{\sqrt{N_0(2k)}} \\
c_1 &= \frac{1}{\sqrt{N_2(2k)}} \\
c_2 &= \frac{1}{\sqrt{N_4(2k) - \frac{N_2^2(2k)}{N_0(2k)}}} \\
c_3 &= \frac{1}{\sqrt{N_6(2k) - \frac{N_4^2(2k)}{N_2(2k)}}}.
\end{aligned} \tag{2.13}$$

Then the ratio $r_i,\ i = 0, 1, 2, ...$ from previous discussion can be easy to calculate

$$r_i = \frac{c_i}{c_{i+1}}. \tag{2.14}$$

## 2.3 Convolution

However, the convolution of two basic functions is hard to obtain. Firstly we define two integrals

$$M_{m,n}(\theta, k_1, k_2) \equiv \int_{-\pi}^{\pi} e^{k_1 \cos(\theta-\theta')} \sin^m(\theta-\theta') e^{k_2 \sin\theta'} \sin^n\theta' d\theta', \tag{2.15}$$

$$T_{m,n}(\theta, k_1, k_2) \equiv \int_{-\pi}^{\pi} e^{k_1 \cos(\theta-\theta')} e^{k_2 \sin\theta'} \sin^m(\theta-\theta') \cos(\theta-\theta') \sin^n\theta' d\theta'. \tag{2.16}$$

Our calculation base on the approximation which assumes the convolution of two von Mises functions is still a von Mises function [7]

$$M_{0,0}(\theta, k_1, k_2) = \int_{-\pi}^{\pi} e^{k_1 \cos(\theta-\theta')} e^{k_2 \sin\theta'} d\theta' \approx \frac{2\pi I_0(k_1) I_0(k_2)}{I_0(k_3)} e^{k_3 \cos\theta}, \tag{2.17}$$

where $k_3 = A^{-1}(A(k_1)A(k_2)),\ A(k) = \frac{I_1(k)}{I_0(k)}$. Take derivative of $M_{0,0}$ with respect to $k_1$, we have $T_{0,0} \approx e^{k_3\cos\theta}\left[F'(k_1) + F\frac{\partial k_3}{\partial k_1}\cos\theta\right]$, where $F(k_1,k_2) = \frac{2\pi I_0(k_1)I_0(k_2)}{I_0(k_3)}$, $\frac{\partial k_3}{\partial k_1} = \frac{A'(k_1)A(k_2)}{A'(k_3)}$, $F'(k_1)$ denotes the derivative of $F(k_1)$ with respect to $k_1$. We can derive those integrals systematically. Take derivative of $M_{m,n}$

$$\frac{\partial M_{m,n}}{\partial\theta} = mT_{m-1,n} - k_1 M_{m+1,n}. \tag{2.18}$$

That allow us to find $M_{m+1,n}$. We take derivative of $T_{m,n}$ with respect to $\theta$ then obtain

$$\frac{\partial T_{m,n}}{\partial\theta} = -k_1 T_{m+1,n} + mM_{m-1,n} - (m+1)M_{m+1,n}. \tag{2.19}$$

We will find $T_{m+1,n}$. Consider the symmetry of $M_{m,n}$ we have

$$M_{m,n}(\theta, k_1, k_2) = M_{n,m}(\theta, k_2, k_1), \tag{2.20}$$

for $T_{m,n}$, we also have

$$\begin{aligned} T_{m,n}(k_1,k_2) &= \int_{-\pi}^{\pi} e^{k_1\cos(\theta-\theta')} e^{k_2\sin\theta'} \sin^m(\theta-\theta')\cos(\theta-\theta')\sin^n\theta' d\theta' \\ &= \cos\theta T_{n,m}(k_2,k_1) + \sin\theta M_{m,n+1}(k_1,k_2), \end{aligned} \tag{2.21}$$

which will allow us to find $M_{m,n}$ and $T_{m,n}$ $m,n = 1,2,...$ starting from $M_{0,0}$ and $T_{0,0}$.

## 2.4 Approximation

Actually this approximation of von Mises convolution may not as accurate as we expect. For instance we know $\int_{-\pi}^{\pi} e^{2k\cos\theta}\sin^2\theta d\theta = N_2(2k) = \frac{\pi I_1(2k)}{k}$, meanwhile $-M_{1,1}(0,k,k) =$

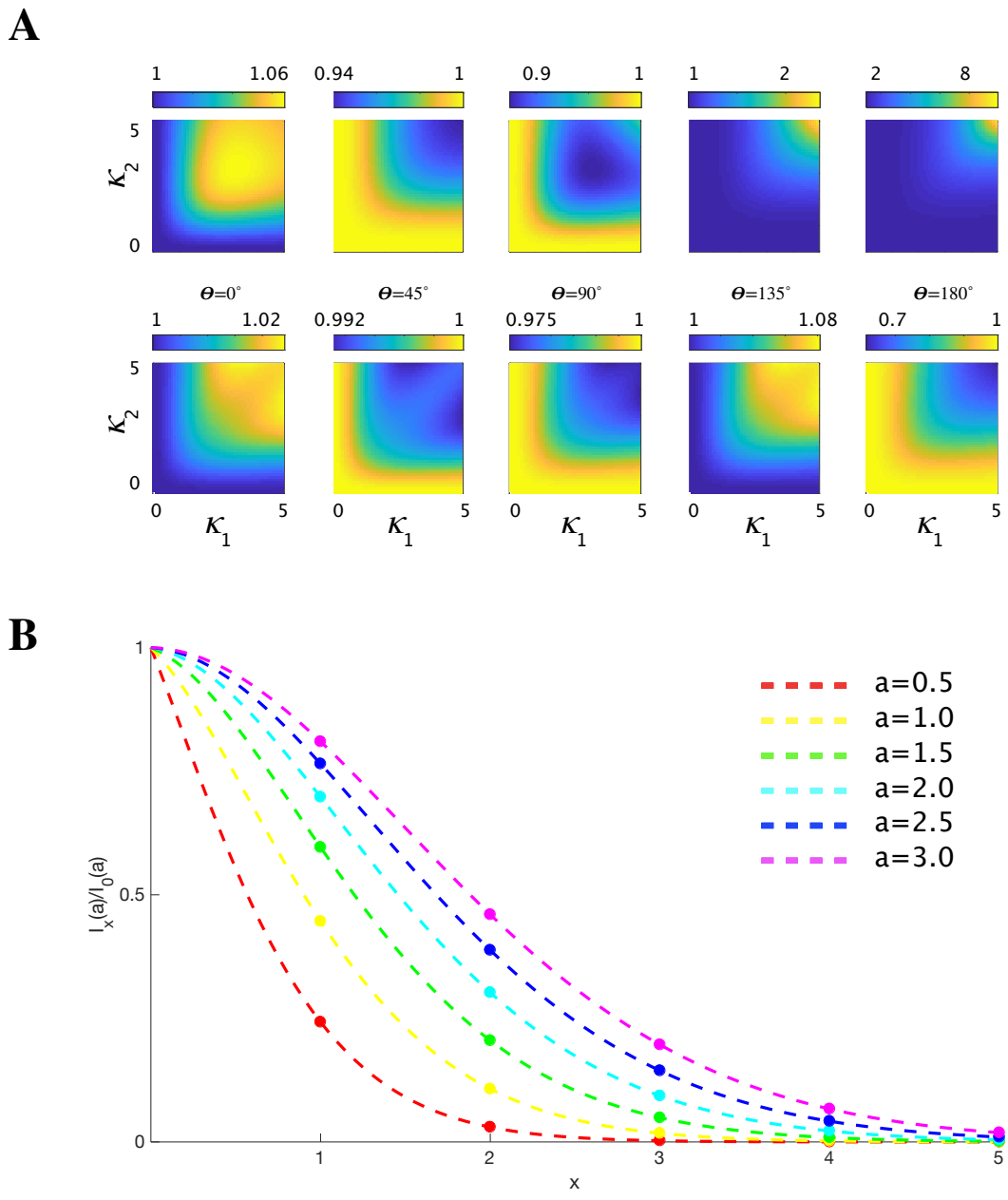


Figure 2.1: Illustration of the approximation and Fourier basis. A: the ratio of estimated value to actual value for previous approximation (first row) and modified approximation (second row) given two concentration ($\kappa_1$, $\kappa_2$) and angular disparity ($\theta$), color indicates the magnitude of the ratio. B: Function $I_x(a)/I_0(a)$ for different width $a$.

$\frac{2\pi k_3 I_0^2(k) e^{k_3}}{k^2 I_0(k_3)}$, where $k_3 = A^{-1}[A(k)^2]$. This percentage error is close to 40% when $2 < k < 3$. It works perfectly when $k$ is approaching infinity.

There are two way to solve the problem. One is to modified this approximation. We know the integral

$$\int_{-\pi}^{\pi} e^{k_1 \cos(\theta-\theta')} e^{k_2 \cos\theta'} d\theta' = 2\pi I_0(\sqrt{k_1^2 + k_2^2 + 2k_1 k_2 \cos\theta}), \tag{2.22}$$

in [7], this Bessel function is approximated by

$$I_0(\sqrt{k_1^2 + k_2^2 + 2k_1 k_2 \cos\theta}) \approx \frac{I_0(k_1) I_0(k_2)}{I_0(k_3)} e^{k_3 \cos\theta}, \ where \ k_3 = A^{-1}[A(k_1)A(k_2)]. \tag{2.23}$$

For convenience, we can take the log of both sides. Note $k = \sqrt{k_1^2 + k_2^2 + 2k_1 k_2 \cos\theta}$. Suppose $\ln(I_0(k))$ could be approximated by $d + h\cos(f\theta)$, we expand $\ln(I_0(k))$, consider first three terms only

$$\ln(I_0(k)) \approx \frac{b_0}{2} + b_1 \cos\theta + b_2 \cos 2\theta, \tag{2.24}$$

where $b_i = \frac{1}{\pi}\langle \ln(I_0(k)), \cos(i\theta)\rangle \ i = 0, 1, 2$. That is, we have

$$\frac{b_0}{2} + b_1 \cos\theta + b_2 \cos 2\theta \approx d + h\cos(f\theta). \tag{2.25}$$

Multiply both sides by $\cos(i\theta), \ i = 0, 1, 2$, integrate over $\theta$, then we get the solution for the coefficients

$$\begin{aligned} f &= \sqrt{\frac{4b_2 + b_1}{b_2 + b_1}} \\ h &= \frac{\pi b_1 (1 - f^2)}{2f \sin(\pi f)} \\ d &= \frac{b_0}{2} - \frac{b_1(1 - f^2)}{2f^2}. \end{aligned} \tag{2.26}$$

Eventually this approximation could be expressed by

$$\int_{-\pi}^{\pi} V(\theta - \theta', k_1) V(\theta', k_2) d\theta' \approx F(k_1, k_2) V(f\theta, k_3). \tag{2.27}$$

Figure 2.1 A shows this approximation is more accurate than previous case if we still want a von Mises form basic functions. Given $k_1$ and $k_2$, we calculate $f, \ h, \ d$ respectively. Note that $F = \frac{e^d}{2\pi I_0(k_1) I_0(k_2)}$ and $k_3 = h$ represent the coefficient and concentration of the result respectively. So the convolution of two von Mises functions is still a von Mises function.

The other way is to switch to Fourier basic functions. When we consider applying Fourier basis to a von Mises function, the coefficient of each order will be $\frac{I_n(a)}{I_0(a)}$, where $a$ is the width of that von Mises function. Figure 2.1 B shows that when $a$ is small, we don't need to take high order perturbation into consideration. Since we are handling the case when the concentration is comparatively small ($a \approx 1.5$), it's more suitable for us to choose Fourier series when applying projection method. For Fourier basis, the zeroth-order perturbation may refer to a constant (shift mode), the first-order perturbation will refer to height mode ($\cos(\theta)$) and position mode ($\sin(\theta)$), and the second-order perturbation refer to width mode ($\cos(2\theta)$) and skewness mode ($\sin(2\theta)$) around the point $a = 1.5$.

# Chapter 3

# Projection Methods for Network Dynamics

## 3.1 Bump Position

Suppose the bump profile $\psi_m$ could be expressed as Fourier series in Eq. (1.5), we multiply both sides of the steady state equations of Eq. (1.1) by 1, $\cos(y - s_m)$, $\cos 2(y - s_m)$, $\sin 2(y - s_m)$ in turn and integrate over $y$ without considering the noise

$$u_{m0} = \frac{\rho J_{rc}}{D_m}\left[u_{m0}^2 + \frac{u_{m1}^2}{2} + \frac{u_{m2}^2}{2} + \frac{u_{m3}^2}{2}\right] + \frac{\rho J_{rp}}{D_{\bar{m}}}\left[u_{\bar{m}0}^2 + \frac{u_{\bar{m}1}^2}{2} + \frac{u_{\bar{m}2}^2}{2} + \frac{u_{\bar{m}3}^2}{2}\right] + \frac{I_m}{2\pi} + I_b, \tag{3.1}$$

$$\begin{aligned} u_{m1} =& \frac{\rho J_{rc}}{D_m} B_1(a_0)\left[2u_{m0}u_{m1} + u_{m1}u_{m2}\right] + \frac{I_m B_1(a_0/2)}{\pi}\cos(x_m - s_m) \\ &+ \frac{\rho J_{rp}}{D_{\bar{m}}} B_1(a_0)\left[(2u_{\bar{m}0}u_{\bar{m}1} + u_{\bar{m}1}u_{\bar{m}2})\cos(s_{\bar{m}} - s_m) - u_{\bar{m}1}u_{\bar{m}3}\sin(s_{\bar{m}} - s_m)\right], \end{aligned} \tag{3.2}$$

$$\begin{aligned} 0 =& \frac{\rho J_{rc}}{D_m} B_1(a_0) u_{m1}u_{m3} + \frac{I_m B_1(a_0/2)}{\pi}\sin(x_m - s_m) \\ &+ \frac{\rho J_{rp}}{D_{\bar{m}}} B_1(a_0)\left[(2u_{\bar{m}0}u_{\bar{m}1} + u_{\bar{m}1}u_{\bar{m}2})\sin(s_{\bar{m}} - s_m) + u_{\bar{m}1}u_{\bar{m}3}\cos(s_{\bar{m}} - s_m)\right], \end{aligned} \tag{3.3}$$

$$\begin{aligned} u_{m2} =& \frac{\rho J_{rc}}{D_m} B_2(a_0)\left[2u_{m0}u_{m2} + \frac{u_{m1}^2}{2}\right] + \frac{I_m B_2(a_0/2)}{\pi}\cos 2(x_m - s_m) \\ &+ \frac{\rho J_{rp}}{D_{\bar{m}}} B_2(a_0)\left[(2u_{\bar{m}0}u_{\bar{m}2} + \frac{u_{\bar{m}1}^2}{2})\cos 2(s_{\bar{m}} - s_m) - 2u_{\bar{m}0}u_{\bar{m}3}\sin 2(s_{\bar{m}} - s_m)\right], \end{aligned} \tag{3.4}$$

$$\begin{aligned} u_{m3} =& \frac{\rho J_{rc}}{D_m} B_2(a_0) 2u_{m0}u_{m3} + \frac{I_m B_2(a_0/2)}{\pi}\sin 2(x_m - s_m) \\ &+ \frac{\rho J_{rp}}{D_{\bar{m}}} B_2(a_0)\left[(2u_{\bar{m}0}u_{\bar{m}2} + \frac{u_{\bar{m}1}^2}{2})\sin 2(s_{\bar{m}} - s_m) + 2u_{\bar{m}0}u_{\bar{m}3}\cos 2(s_{\bar{m}} - s_m)\right], \end{aligned} \tag{3.5}$$

where $D_m = 1 + \pi\omega\rho[2u_{m0}^2 + u_{m1}^2 + u_{m2}^2 + u_{m3}^2 + J_{int}(2\bar{u}_{\bar{m}0}^2 + \bar{u}_{\bar{m}1}^2 + \bar{u}_{\bar{m}2}^2 + \bar{u}_{\bar{m}3}^2)]$ and $B_n(k) = \frac{I_n(k)}{I_0(k)}$. The estimated heading direction is encoded in neural activities, that is, the firing rate of neurons $R_m(y,t)$ is used to calculate the bump position $\hat{s}_m$

$$\hat{s}_m = \arg(\sum_{y=-\pi}^{\pi} R_m(y,t)e^{jy}), \tag{3.6}$$

where $j$ is the imaginary unit. The estimated heading direction $\hat{s}_m$ can be expressed by other parameters

$$\hat{s}_m = \text{atan2}[(2u_{m0}+u_{m2})\sin(s_m)+u_{m3}\cos(s_m), (2u_{m0}+u_{m2})\cos(s_m)-u_{m3}\sin(s_m)]. \tag{3.7}$$

We compare analytic results with simulation in Fig. 3.1. Since our calculation is involved in high order modes, specific physical features could be captured in analytic results, including the shift, the height, the position, the width and the skewness of a bump profile. Note $\Delta x \equiv x_2 - x_1$ is the angular disparity of two cues. When $\Delta x > 90^\circ$ we only need to reverse the order of congruent and opposite groups because of the symmetry. All parameters are given in the Chapter 4 for strong input case except here we set $J_{int} = 0.5$ which is given in [1]. The time step size is $0.01\tau$ and each time period is set equal to $100\tau$ to make sure the solution has already converged. We are using Euler method to solve dynamic equations in our simulation.

## 3.2 Noise Variance

Next step we need take noise into consideration. In [1], the dynamics of congruent groups of neurons in the presence of noise can by approximated by

$$\begin{aligned}\tau\frac{\partial\psi_m(y)}{\partial t} =& -\psi_m(y) + \frac{J_{rc}}{D_m}\int_{-\pi}^{\pi} V(y-y',a_0)\psi^2(y') + \frac{J_{rp}}{D_{\bar{m}}}\int_{-\pi}^{\pi} V(y-y',a_0)\bar{\psi}^2(y') \\ &+ I_m V(y-x,\frac{a_0}{2}) + I_b + \sqrt{F_0 I_m V(y-x,\frac{a_0}{2})}\xi_m(y,t) + \sqrt{F_0 I_b}\epsilon_m(y,t),\end{aligned} \tag{3.8}$$

where $F_0$ is the Fano factor, $\xi_m$ and $\epsilon_m$ are Gaussian white noise of zero mean and variance satisfying $\langle \xi_m(y,t), \xi_{m'}(y',t')\rangle = \delta_{mm'}\delta(y-y')\delta(t-t')$ and $\langle \epsilon_m(y,t), \epsilon_{m'}(y',t')\rangle = \delta_{mm'}\delta(y-y')\delta(t-t')$.

Consider the dynamics of displacement mode and multiply both sides by $\sin(y_m - s_m)$,

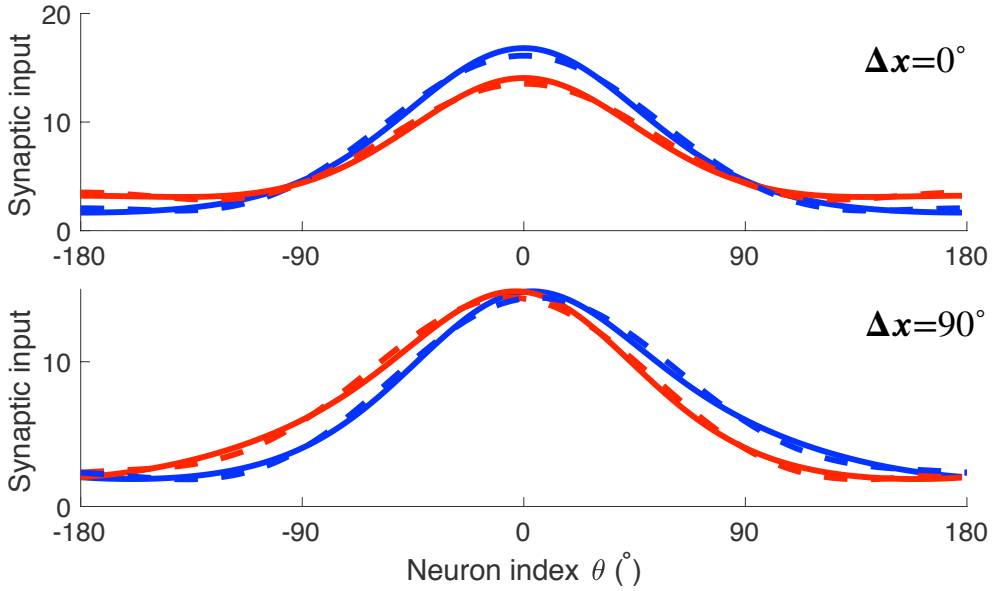


Figure 3.1: Bump profiles (synaptic inputs) of congruent and opposite groups in module 1 without noise. The blue and red colors represent congruent and opposite groups respectively. Solid lines: simulation results, dashed lines: analytic results by using projection method.

integrate over $y_m$

$$\begin{aligned}\tau\frac{\partial}{\partial t}\delta s_m &= -\delta s_m + \frac{\rho J_{rc}}{D_m u_{m1}} B_1(a_0)\left[2u_{m0}u_{m1} + u_{m1}u_{m2}\right]\delta s_m \\ &+ \frac{\rho J_{rp}}{D_{\bar{m}} u_{m1}} B_1(a_0)\left[(2u_{\bar{m}0}u_{\bar{m}1} + u_{\bar{m}1}u_{\bar{m}2})\cos(s_{\bar{m}} - s_m) - u_{\bar{m}1}u_{\bar{m}3}\sin(s_{\bar{m}} - s_m)\right]\delta s_{\bar{m}} \\ &+ \frac{\sqrt{F_0 I_m}}{\pi u_{m1}}\int\sqrt{V(y_m - x_m, a_0/2)}\sin(y_m - s_m)\xi_m dy_m + \frac{\sqrt{F_0 I_b}}{\pi u_{m1}}\int\sin(y_m - s_m)\epsilon_m dy_m.\end{aligned} \tag{3.9}$$

The equivalent noise temperature is given by

$$\begin{aligned}T_m &= \frac{F_0}{2\pi^2\rho u_{m1}^2}\left[I_m\int V(y_m - x_1 m, a_0/2)\sin^2(y_m - s_m)dy_m + I_b\int\sin^2(y_m - s_m)dy_m\right] \\ &= \frac{F}{2\pi^2\rho u_{m1}^2}\left[(\frac{I_m}{2} + \pi I_b) - \frac{I_m}{2}B_2(a_0/2)\cos 2(x_m - s_m)\right].\end{aligned} \tag{3.10}$$

Here we can prove the heading direction $s_m$ is a Gaussian, consider the dynamics $\tau\frac{\partial x_i}{\partial t} = -\Sigma_j g_{ij}x_j + \xi_j$, where $\langle\xi_i(t)\xi_j(t')\rangle = 2T_i\delta_{ij}\delta(t = t')$ and $\langle\xi_i(t)\rangle = 0$. Diagonalizing the matrix, $g_{ij} = \Sigma_k S_{ik}\lambda_k S^{-1}_{kj}$. Then

$$\tau\frac{\partial}{\partial t}\Sigma_j S^{-1}_{ij}x_j = -\lambda_i\Sigma_j S^{-1}_{ij}x_j + \Sigma_j S^{-1}_{ij}\xi_j, \tag{3.11}$$

the solution is

$$x_i(t) = \Sigma_j S_{ij}\int_{-\infty}^{t}\frac{dt'}{\tau}\exp[-\frac{\lambda_j}{\tau}(t - t')]S^{-1}_{jk}\xi_k(t'). \tag{3.12}$$

Consider the moments of the distribution of $x_i(t)$

$$\langle x_i^2(t)\rangle = \Sigma_{j_1\ldots j_{2k}k_1\ldots k_{2k}} S_{ij_1}\ldots S_{ij_{2n}} \int_{-\infty}^{t} \frac{dt_1}{\tau} \exp[-\frac{\lambda_{j_1}}{\tau}(t-t_1)]$$
$$\ldots \int_{-\infty}^{t} \frac{dt_{2n}}{\tau} \exp[-\frac{\lambda_{j_{2n}}}{\tau}(t-t_{2n})] S^{-1}_{j_1k_1}\ldots S^{-1}_{j_{2n}k_{2n}} \langle \xi_{k(t_1)}\ldots\xi_{k_{2n}}(t_{2n})\rangle. \tag{3.13}$$

The number of ways the pairing of the noise terms can be done is $(2n)!/(2!^n n!) = (2n-1)!!$. Hence

$$\langle x_i^2(t)\rangle = (2n-1)!!\{\Sigma_{j_1j_2k_1k_2} S_{ij_1}S_{ij_2} \int_{-\infty}^{t} \frac{dt_1}{\tau} \exp[-\frac{\lambda_{j_1}}{\tau}(t-t_1)]$$
$$\int_{-\infty}^{t} \frac{dt_2}{\tau} \exp[-\frac{\lambda_{j_2}}{\tau}(t-t_2)] S^{-1}_{j_1k_1} S^{-1}_{j_2k_2} 2T_{k_1}\delta_{k_1k_2}\delta(t_1-t_2)\}^n, \tag{3.14}$$

after integrating

$$\langle x_i^2(t)\rangle = (2n-1)!! \left[\Sigma_{ijk} S_{ij}S_{ik} \frac{2T_l}{(\lambda_j+\lambda_k)\tau} S^{-1}_{jl} S^{-1}_{kl}\right]^n. \tag{3.15}$$

So the distribution of $x_i(t)$ is a Gaussian with variance

$$\sigma_i^2 = \Sigma_{ijk} S_{ij}S_{ik} \frac{2T_l}{(\lambda_j+\lambda_k)\tau} S^{-1}_{jl} S^{-1}_{kl}. \tag{3.16}$$

The concentration $\kappa_m = \frac{1}{\sigma_m^2}$ for the matrix $G_{ij},\ i,j=1,2$, where

$$\sigma_m^2 = \frac{T_m}{(G_{mm}+G_{\bar{m}\bar{m}})\tau} + \frac{T_m G^2_{\bar{m}\bar{m}} + T_{\bar{m}} G^2_{m\bar{m}}}{(G_{mm}G_{\bar{m}\bar{m}} - G_{m\bar{m}}G_{\bar{m}m})(G_{mm}+G_{\bar{m}\bar{m}})\tau}. \tag{3.17}$$

# Chapter 4

# Bayesian Inference

## 4.1 Incompleteness of Old Model

We firstly focus on the case that two stimulus strengths are equal, that is $I_m = I_{\bar{m}} = I$, furthermore, $D_m = D_{\bar{m}} = D$, $u_{mn} = u_{\bar{m}n} = u_n$, $T_m = T_{\bar{m}} = T$. The equivalent noise temperature and the coefficient of the height mode of opposite groups of neurons will be denoted as $\bar{T}$ and $\bar{u}_1$ respectively. We consider competition between congruent and opposite groups in module $m$. The solution is symmetric with respect to the perception displacement, that is, $s_m - x_m = x_{\bar{m}} - s_{\bar{m}}$. We have $G_{mm} = G_{\bar{m}\bar{m}}$, $G_{m\bar{m}} = G_{\bar{m}m}$, $\bar{G}_{mm} = \bar{G}_{\bar{m}\bar{m}}$, $\bar{G}_{m\bar{m}} = \bar{G}_{\bar{m}m}$ because of symmetry. The noise temperature are given below

$$T = \frac{F_0}{2\pi^2\rho u_1^2}\left[\frac{I}{2}(1 - B_2(a_0/2)\cos 2(x_m - s_m)) + \pi I_b)\right], \tag{4.1}$$

$$\bar{T} = \frac{F_0}{2\pi^2\rho \bar{u}_1^2}\left[\frac{I}{2}(1 - B_2(a_0/2)\cos 2(x_m - \bar{s}_m)) + \pi I_b)\right]. \tag{4.2}$$

The concentration of congruent groups of neurons could be approximate by

$$\hat{\kappa}_m = \frac{1}{\sigma_m^2} = \frac{\tau}{T}(G_{mm} - \frac{G_{m\bar{m}}^2}{G_{mm}}) \approx \frac{\tau}{T}. \tag{4.3}$$

Hence $\frac{\hat{\kappa}_m}{\hat{\bar{\kappa}}_m} \approx \frac{u_1^2}{\bar{u}_1^2}$. The information of bump position and noise variance of neural activities is decoded from Eqs. (3.2) and (3.3), which could be simplified (the congruent group of neurons in module 1)

$$1 = HJ_{rc} + HJ_{rp}\cos\Delta s + \frac{F}{u_1}\cos(x_1 - s_1) \tag{4.4}$$

$$0 = HJ_{rp}\sin\Delta s + \frac{F}{u_1}\sin(x_1 - s_1), \tag{4.5}$$

where $\Delta s \equiv s_2 - s_1$, $H = \frac{\rho}{D}(2u_0 + u_2)B_1(a_0)$, $F = \frac{IB_1(a_0/2)}{\pi}$, in weak input limit $H$ can be treated as a constant. When $\Delta s = \frac{\pi}{2}$, $|s_m - x_m|$ will reach the maximum, Eqs. (4.4)

and (4.5) will become

$$1 = HJ_{rc} + \frac{F}{u_1} \tag{4.6}$$

$$0 = HJ_{rp} + \frac{F}{u_1}(x_1 - s_1), \tag{4.7}$$

since $(x_1 - s_1) \to 0$, we have $(s_1 - x_1)_{\Delta s=\frac{\pi}{2}} = \frac{HJ_{rp}}{1-HJ_{rc}}$. When $\Delta x = 0$, then $x_m = s_m$, Eq. (4.4) will become

$$1 = HJ_{rc} + HJ_{rp} + \frac{F}{u_1}. \tag{4.8}$$

However, $HJ_{rp}$ is small, the ratio of $u_1$ to $\bar{u}_1$ can be approximated by

$$\left(\frac{u_1}{\bar{u}_1}\right)_{\Delta x=0} = \frac{1 - HJ_{rc} + HJ_{rp}}{1 - HJ_{rc} - HJ_{rp}} \approx 1 + \frac{2}{1 - HJ_{rc}} HJ_{rp} = 1 + 2(s_1 - x_1)_{\Delta s=\frac{\pi}{2}}, \tag{4.9}$$

then we have the following approximation for the concentrations of the neural activities of the congruent and opposite groups of neurons

$$\left(\frac{\hat{\kappa}_1 - \hat{\bar{\kappa}}_1}{\hat{\kappa}_1 + \hat{\bar{\kappa}}_1}\right)_{\Delta x=0} = \frac{\left(\frac{u_1^2}{\bar{u}_1^2}\right)_{\Delta x=0} - 1}{\left(\frac{u_1^2}{\bar{u}_1^2}\right)_{\Delta x=0} + 1} \approx 2(s_1 - x_1)_{\Delta s=\frac{\pi}{2}}. \tag{4.10}$$

That is, in weak input limit, if we are going to fit the variance in this network, the angle decoded from population vector will be twice as large as the real angle. However, this ratio is always greater than 2 when input strength is in normal range.

## 4.2 Output-Dependent Noise

In order to implement Bayesian prediction, we define the length of population vector $\hat{A} \equiv \mod\left(\frac{1}{N}\sum_{y=-\pi}^{\pi} R_m(y)e^{jy}\right) = \frac{\rho}{ND} u_1 \sqrt{(2u_0 + u_2)^2 + u_3^2}$, where $j$ is the imaginary unit. In contrast with the noise in [1], we rewrite the noise term: $\sqrt{F_0 \hat{A}}\epsilon_m$. Although we only slightly change the noise expression, it can be helpful since the new equivalent noise temperatures will be

$$T = \frac{\sqrt{(2u_0 + u_2)^2 + u_3^2}}{2\pi N D u_1} F_0, \tag{4.11}$$

$$\bar{T} = \frac{\sqrt{(2\bar{u}_0 + \bar{u}_2)^2 + \bar{u}_3^2}}{2\pi N \bar{D} \bar{u}_1} F_0. \tag{4.12}$$

In weak input limit, the coefficients of high order modes ($u_2$ and $u_3$) will vanish, and $u_0 \approx \bar{u}_0$. In this case,

$$\hat{\kappa}_m \approx \frac{\pi\tau N D}{F_0 u_0} u_1, \tag{4.13}$$

$$\hat{\bar{\kappa}}_m \approx \frac{\pi\tau N \bar{D}}{F_0 \bar{u}_0} \bar{u}_1. \tag{4.14}$$

That is, $\hat{\kappa}_m \approx c_0 u_1$ and $\hat{\bar{\kappa}}_m \approx c_0 \bar{u}_0$, where $c_0$ denotes the coefficient of $u_1$ and $\bar{u}_1$. From Eq. (4.4) we have

$$\begin{aligned} \left(\frac{F}{u_1}\right)^2 =& (1 - HJ_{rc})^2 + (HJ_{rp})^2 - 2(1 - HJ_{rc})HJ_{rp}\cos\Delta s, \\ u_1^2 =& \frac{F^2}{(1 - HJ_{rc})^2 + (HJ_{rp})^2 - 2(1 - HJ_{rc})HJ_{rp}\cos\Delta s}. \end{aligned} \tag{4.15}$$

Actually $HJ_{rp}$ is small, and $\cos\Delta s = \cos[\Delta x - 2(s_1 - x_1)] \approx \cos\Delta x$. We expand $\tan(s_1 - x_1)$ and $u_1^2$ then obtain

$$\begin{aligned} \tan(s_1 - x_1) =& \frac{HJ_{rp}\sin\Delta s}{1 - HJ_{rc} - HJ_{rp}\cos\Delta s} \\ \approx& \frac{HJ_{rp}\sin\Delta s}{1 - HJ_{rc}} \\ \approx& \frac{HJ_{rp}\sin\Delta x}{1 - HJ_{rc} + HJ_{rp}\cos\Delta x}, \end{aligned} \tag{4.16}$$

$$\begin{aligned} u_1^2 \approx& \frac{F^2}{(1 - HJ_{rc})^2} + \frac{2F^2 HJ_{rp}}{1 - HJ_{rc})^3}\cos\Delta s \\ =& \frac{F^2}{(1 - HJ_{rc})^4}\left[(1 - HJ_{rc})^2 - 2HJ_{rp}(1 - HJ_{rc})\cos(\pi - \Delta s)\right] \\ \approx& \frac{F^2}{(1 - HJ_{rc})^4}\left[(1 - HJ_{rc})^2 - 2HJ_{rp}(1 - HJ_{rc})\cos(\pi - \Delta x) + (HJ_{rp})^2\right]. \end{aligned} \tag{4.17}$$

Finally we have

$$\tan(s_1 - x_1) \approx \frac{HJ_{rp}\sin\Delta x}{1 - HJ_{rc} + HJ_{rp}\cos\Delta x}, \tag{4.18}$$

$$\hat{\kappa}_m^2 \approx \frac{c_0^2 F^2}{(1 - HJ_{rc})^4}\left[(1 - HJ_{rc})^2 - 2HJ_{rp}(1 - HJ_{rc})\cos(\pi - \Delta x) + (HJ_{rp})^2\right], \tag{4.19}$$

for combined case. When $I_1 = I$ and $I_2 = 0$, this network is asymmetric. The bump in module 2 is much weaker so we can ignore the input from the other module and find the concentration decoded from module 1 is $\hat{\kappa}_1 = \frac{c_0 F}{(1 - HJ_{rc})}$. When $I_2 = I$ and $I_1 = 0$,

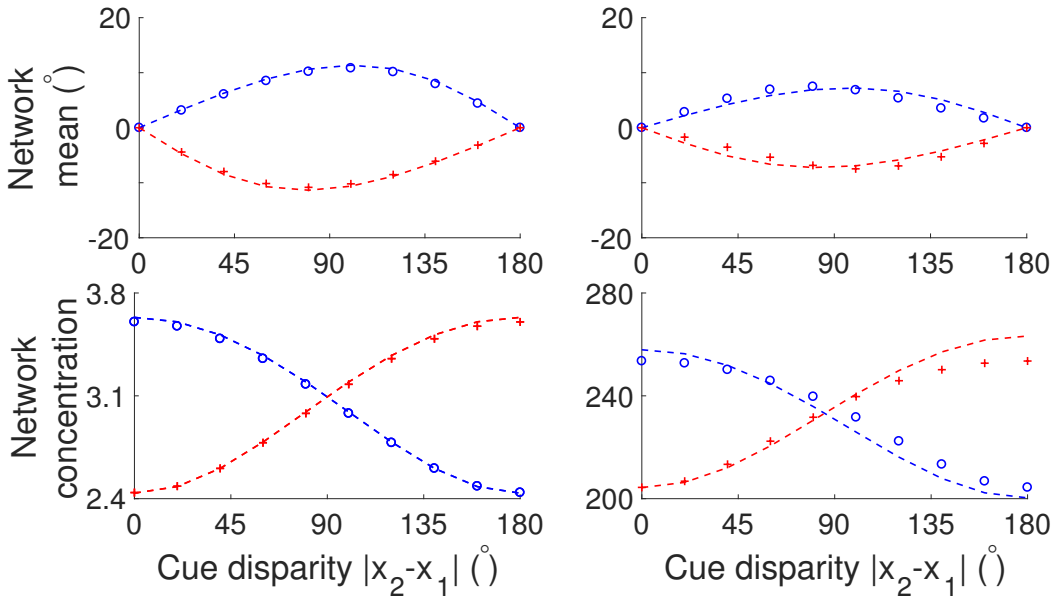


Figure 4.1: Weak input ($I_1 = I_2 = 0.01U_0$, left column) and strong input ($I_1 = I_2 = 0.7U_0$, right column). Symbols: network results; dashed lines: Bayesian prediction. The blue and red colors represent congruent and opposite groups in module 1 respectively.

the concentration decoded from module 1 is $\hat{\kappa}_{2s} = \frac{c_0 FHJ_{rp}}{(1-HJ_{rc})^2}$ based on previous discussion. Compare the results, we will have $\hat{\kappa}_1 e^{j\hat{s}_1}|_{I_1,I_2} = \hat{\kappa}_1 e^{jx_1}|_{I_1} + \hat{\kappa}_{2s} e^{jx_2}|_{I_2}$, where $j$ is the imaginary unit. Similarly, for opposite groups we also have $\hat{\tilde{\kappa}}_1 e^{j\hat{s}_1}|_{I_1,I_2} = \hat{\tilde{\kappa}}_1 e^{jx_1}|_{I_1} - \hat{\tilde{\kappa}}_{2s} e^{j(x_2)}|_{I_2}$.

## 4.3 Results of Modified Noise Variance

Consider the task of inferring the stimuli $s_m$ ($m = 1,\ 2$) from the received cues $x_m$ ($m = 1,\ 2$). It has been shown that for uniform distributions of $s_m$ and cues $x_m$, the condition for the network to produce Bayesian inference is that the marginal posterior distribution of $s_1$ conditional on the direct cue $x_1$ and indirect cue $x_2$ is given by [1]

$$p(s_1|x_1, x_2) \propto p(s_1|x_1)p(s_1|x_2), \tag{4.20}$$

where the marginal posterior distribution $p(s_1|x_2)$ given the indirect cue $x_2$ depends on the prior distribution $p(s_1, s_2)$ via

$$p(s_1|x_2) \propto \int ds_2 p(x_2|s_2)p(s_1, s_2). \tag{4.21}$$

The expressions of the marginal posterior distribution of $s_2$ can be obtained by interchanging $s_1$ and $s_2$; hereafter we will focus on the result for $s_1$. To explain the role of

congruent and opposite neurons, it is convenient to consider likelihood distributions in the form of the von Mises distribution with concentration $\kappa_m$,

$$p(x_m|s_m) = V(x_m - s_m, \kappa_m). \tag{4.22}$$

Hence, to verify whether the congruent groups of the proposed network is able to make Bayesian predictions, one may use them to estimate the posterior distributions of $s_1$ when it receives cue 1 only, cue 2 only, and cues 1 and 2 combined, and test whether the result of the combined cues agrees with those predicted from the single cues according to Eq. (4.20).

We first consider a prior that the stimuli $s_1$ and $s_2$ are correlated. In particular, we consider the prior

$$p(s_1, s_2) = V(s_1 - s_2, \kappa_s). \tag{4.23}$$

When this von Mises prior is substituted into Eq. (7), the integration yields a new von Mises function $V(s_1 - x_2, \kappa_{2s})$, where $\kappa_{2s} \equiv A^{-1}[A(\kappa_2)A(\kappa_s)]$ with the function $A$ related to the modified Bessel functions via $A(\kappa) \equiv I_1(\kappa)/I_0(\kappa)$ [7]. In turn, when Eq. (4.21) is substituted into Eq. (4.20), the product of two von Mises distributions yields another von Mises distribution whose mean and concentration are given by a vector sum rule. Thus, the condition (4.20) for Bayesian inference reduces to

$$\hat{\kappa}_1 e^{j\hat{s}_1}|_{I_1,I_2} = \hat{\kappa}_1 e^{j\hat{s}_1}|_{I_1} + \hat{\kappa}_{2s} e^{j\hat{s}_2}|_{I_2}. \tag{4.24}$$

The subscripts represent the non-vanishing stimuli applied to the network, and the hat accents represent the network estimates.

To segregate the information from the two cues, we consider the disparity information of stimulus 1 defined to be

$$p_d(s_1|x_1, x_2) \propto \frac{p(s_1|x_1)}{p(s_1|x_2)}. \tag{4.25}$$

Noting that the cosine function satisfies $\cos(y - y' - \pi) = -\cos(y - y')$, we obtain

$$p_d(s_1|x_1, x_2) \propto V(s_1 - x_1, \kappa_1)V(s_1 - x_2 - \pi). \tag{4.26}$$

Hence, the mean $\Delta\hat{s}_1$ and concentration $\Delta\hat{\kappa}_1$ of the disparity information, to be estimated by the opposite groups of neurons, are given by

$$\hat{\kappa}_1 e^{j\hat{s}_1}|_{I_1,I_2} = \hat{\kappa}_1 e^{j\hat{s}_1}|_{I_1} - \hat{\kappa}_{2s} e^{j\hat{s}_2}|_{I_2}. \tag{4.27}$$

Equations (4.24) and (4.27) are used to generate Bayesian predictions based on the single-input estimates and compare with the combined estimates generated from network simulations (the estimated concentration will be compared with the inverse of the variance). As shown in Fig. 4.1, we find that the network can implement Bayesian inference in the weak input limit. When the inputs are strong, the network prediction starts to deviate from the Bayesian inference, but the estimates remain reasonably close. In contrast, in the original model of Zhang et al., $s_m$ and $\kappa_m$ cannot be estimated accurately simultaneously. This shows that the incorporation of $\hat{A}$ in the noise amplitude improves the accuracy of Bayesian prediction.

All parameters are listed. Each network consists of $N = 180$ congruent and opposite neurons respectively. The connection width $a_0 = 3$ and the time step is $0.01\tau$ using Euler method where $\tau$ is rescaled to 1. The strength of background input is $I_b = 1$. The strength of divisive normalization $\omega = 3 \times 10^{-4}$. Fano factor is denoted as $F_0$ in the noise term, and we set $F_0$ to 0.5. In simulation we fix $x_1 = 0$, that is, $\Delta x \equiv x_2 - x_1 = x_2$. $J_c$ is the threshold recurrent strength for spontaneous bump formation and we choose $J_{rc} = 0.3J_c$ and $J_{rp} = 0.15J_c$. $J_c$ can be found by solving the dynamic equations, which is given by $J_c = \sqrt{\frac{8\pi I_0(a_0/2)^2\omega(1+J_{int})}{I_0(a_0)\rho}}$ and $U_0$ is its corresponding synaptic bump height $U_0 = \frac{J_c e^{a_0/2}}{2\pi\omega(1+J_{int})I_0(a_0/2)}$.

We compare the cases of weak input $I = 0.01U_0$ (left column) and strong input $I = 0.7U_0$ (right coulmn) in module 1. Figure 4.1 shows this network could implement Bayesian inference in weak input limit. When external inputs are strong, the prediction from this network is close to the Bayesian way. However, an independent prior should be included in our model when applying Bayesian prediction.

# Chapter 5

# Priors with an Independent Component

## 5.1 Network Model

So far we have considered the prior in Eq. (4.22) in which the two stimuli are correlated. However, there are many other scenarios described by priors with an additional independent component. Those priors are often used in causal inference tasks, in which the subject is required to determine whether the two cues originate from the same stimulus or they are independent [8, 9]. Hence, we consider the following two-component prior,

$$p(s_1, s_2) = \frac{p_0}{2\pi} V(s_1 - s_2, \kappa_s) + \frac{1 - p_0}{(2\pi)^2}. \tag{5.1}$$

Using Eq. (4.21), the marginal posterior distribution $p(s_1|x_2)$ becomes

$$p(s_1|x_1, x_2) = p_0 C V(s_1 - x_1, \kappa_1) V(s_1 - x_2, \kappa_{2s}) + (1 - p_0) V(s_1 - x_1, \kappa_1), \tag{5.2}$$

where $C$ is the normalization constant. Hence, we add another layer of neurons to represent the posterior taking account of the two components of the prior. The second layer receives the input from congruent neurons (representing the first term in Eq. (5.2)), and the feedforward inputs from the cue (corresponding to the second term in Eq. (5.2)). The dynamics of this group of neurons is given by

$$\begin{aligned} \tau \frac{\partial \psi_{2m}(y,t)}{\partial t} = & -\psi_{2m}(y,t) + \sum_{y'=-\pi}^{\pi} J_{rc} V(y - y', a_0) R_{2m}(y', t) \\ & + p_0 \sum_{y'=-\pi}^{\pi} c_k \cos(y - y') R_m(y', t) + I_m^{ext}(y, t). \end{aligned} \tag{5.3}$$

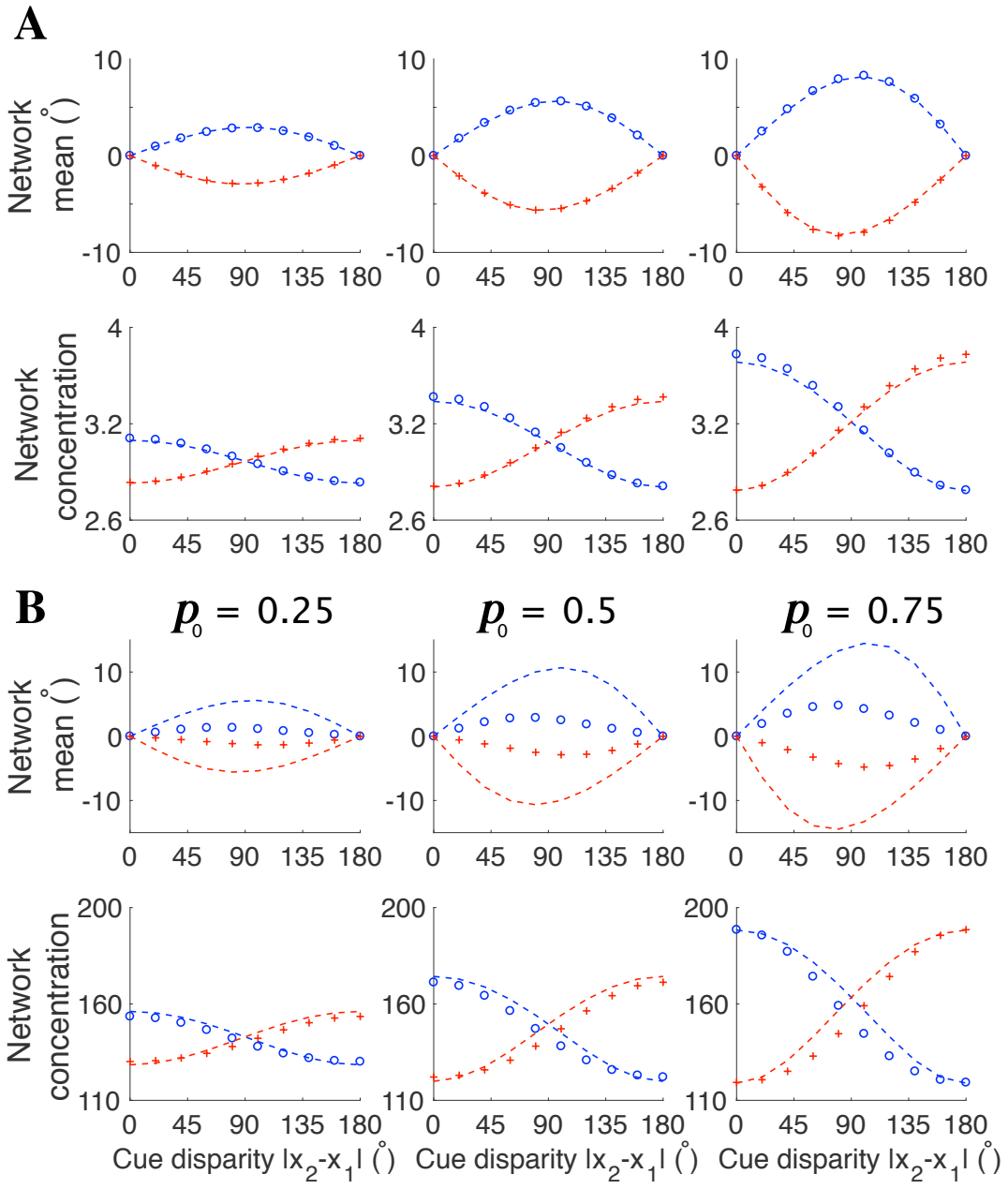


Figure 5.1: Outputs from second layer with varying probability $p_0$. Illustration of the population response of congruent and opposite groups in module 1 applying weak inputs (A) and strong inputs (B). Symbols: network results; dashed lines: Bayesian prediction. The blue and red colors represent congruent and opposite groups in module 1 respectively.

Similarly, we project the steady state equation of Eq. (5.3) onto height and position modes. Consider the dynamics of the congruent group in module 1,

$$1 = H'J_{rc} + (1-p_0)\frac{F}{u_1'}\cos(x_1 - s_1') + p_0\frac{c_k\rho u_1}{Du_1'}\left[(2u_0+u_2)\cos(s_1-s_1') - u_3\sin(s_1-s_1')\right], \tag{5.4}$$

$$0 = (1-p_0)\frac{F}{u_1'}\sin(x_1 - s_1') + p_0\frac{c_k\rho u_1}{Du_1'}\left[(2u_0+u_2)\sin(s_1-s_1') + u_3\cos(s_1-s_1')\right], \tag{5.5}$$

where $H' = \frac{\rho J_{rc}}{D'}(2u_0' + u_2')B_1(a_0)$, $F = \frac{IB_1(a_0/2)}{\pi}$, consider the weak input limit, we know the solution is

$$u_1' = (1-p_0)\frac{F}{1-H'J_{rc}}\cos(x_1 - s_1') + p_0\frac{c_kHu_1}{J_{rc}B_1(a_0)(1-H'J_{rc})}\cos(s_1 - s_1'), \tag{5.6}$$

$$0 = (1-p_0)\frac{F}{1-H'J_{rc}}\sin(x_1 - s_1') + p_0\frac{c_kHu_1}{J_{rc}B_1(a_0)(1-H'J_{rc})}\sin(s_1 - s_1'). \tag{5.7}$$

That is, for combined case $u_1'e^{js_1'} = (1-p_0)\frac{F}{1-H'J_{rc}}e^{jx_1} + p_0\frac{c_kHu_1}{J_{rc}B_1(a_0)(1-H'J_{rc})}e^{js_1}$. Note that the position and the coefficient of height mode of the second layer are denoted as $s_1'$ and $u_1'$ respectively. The neuron groups in the second layer do not have reciprocal connections from the other module. Hence, their output will be the weighted sum of the two types of input. Thus, for the case of combined cues, the output of the congruent group in module 1 will become $p_0\hat{\kappa}_1 e^{j\hat{s}_1}|_{I_1,I_2} + (1-p_0)\kappa_1' e^{jx_1}$ for an appropriate choice of $c_k$, where $\kappa_1'$ is the concentration of the output from the neuron group in the second layer. Meanwhile, $\kappa_1'$ does not vary when this network only receives direct stimulus 1. The output will then be $p_0\hat{\kappa}_1 e^{jx_1}|_{I_1} + (1-p_0)\kappa_1' e^{jx_1}$. When the network only receives stimulus 2, the final output of the congruent group will be $p_0\hat{\kappa}_{2s}e^{jx_2}|_{I_2}$. So in summary, the network has a Bayesian behaviour in all cases.

In Fig. 5.1 we compare the network behaviour in weak and strong inputs, corresponding to $I = 0.01U_0$ and $I = 0.7U_0$ respectively. The outputs from the second layer behave in a Bayesian way in the weak input limit. Although the prior is the sum of two von Mises functions, the output is not double-peaked since the position disparity between inputs from the first layer and the external cue is small.

## 5.2 Vector Space

The vectors, which are corresponding to prior distribution, contain both position and variance information. In weak input limit, we can set $c_k = \frac{J_{rc}+J_{rp}}{1-\sqrt{1-4\rho(J_{rc}+J_{rp})}}$. Fig. 5.2

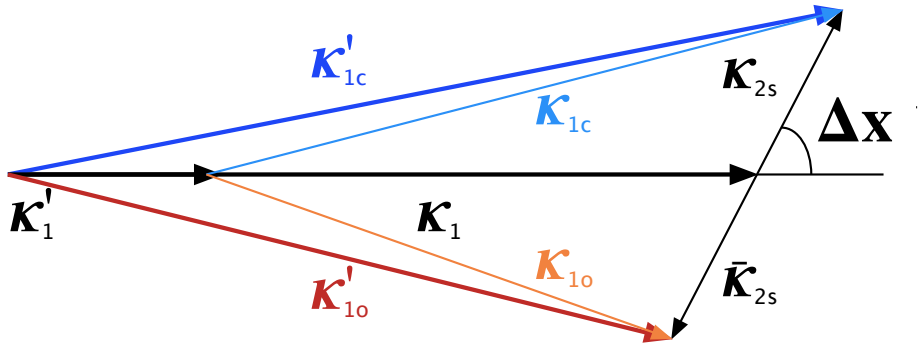


Figure 5.2: Geometric interpretation of vector space. Colored vectors represent the sum of other vectors (black). Outputs from first layer: $\kappa_{1c}$ (congruent) and $\kappa_{1o}$ (opposite), second layer: $\kappa'_{1c}$ (congruent) and $\kappa'_{1o}$ (opposite). Note that the vectors (black) have been rescaled by $p_0$ and $1-p_0$.

shows the vector diagram for achieving information integration. An interesting story is about causal inference, when $J_{rc}$ is small, we have $\frac{|\hat{\kappa}_1|}{|\kappa'_1|} \approx \frac{p_0}{1-p_0}$. If we extract information from two layers, the probability of a common source $p_0$ could calculate from the vector diagram

$$\hat{p}_0 = 1 - \frac{|\kappa'_{1c}|\cos s'_1 - |\kappa_{1c}|\cos s_1}{\lambda|\kappa'_{1o}|\cos \bar{s}'_1 + |\kappa'_{1c}|\cos s'_1}(\lambda+1), \tag{5.8}$$

where $\lambda = -\frac{|\kappa'_{1c}|\sin s'_1}{|\kappa'_{1o}|\sin \bar{s}'_1}$, $1-\hat{p}_0$ corresponds to the probability of two cues coming from the different source. Hence opposite groups are important to distinguish whether two cues are the same or different. The correlation between prediction $\hat{p}_0$ and given $p_0$ has been shown in Fig. 5.3.

## 5.3 Information Segregation

In our model, the prior

$$p(s_1, s_2) = \frac{p_0}{2\pi}V(s_1 - s_2, -\kappa_s) + \frac{1-p_0}{(2\pi)^2}, \tag{5.9}$$

which has been used to describe the correlation for opposite groups of neurons, is not equivalent to what has been used in [10]. However, it includes the same amount of segregation information. Using Eq. (4.25), the inverse of the disparity information is given by

$$p_d(s_1|x_1,x_2)^{-1} = p_0 CV(s_1 - x_2, \kappa_{2s})V(s_1 - x_1 + \pi, \kappa_1) + (1-p_0)V(s_1 - x_1 + \pi, \kappa_1), \tag{5.10}$$

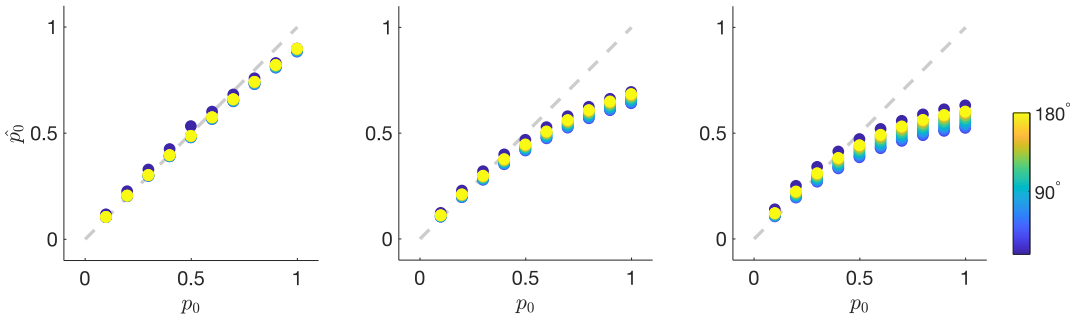


Figure 5.3: Outputs from second layer with varying input strength. From left to right, $I = 0.01U_0,\ 0.05U_0,\ 0.09U_0$. Colormap: color indicates the disparity $\Delta x$ of two cues.

where $C$ is the normalization constant. Note that the stimulus position is shifted by $\pi$ for the opposite group. Hence, we see that the opposite group in the second layer have the same structure as that of the congruent group, except that the positions of the outputs from the second layer are shifted by $\pi$. Fig. 5.1 shows that the disparity information agrees with Bayesian prediction accurately in the weak input limit.

# Chapter 6

# Conclusion

## 6.1 Bayesian Model

Our new model has been shown in Fig. 6.1. In this report we have analyzed the dynamics of neural circuits for multisensory integration and segregation using separate modules for each stimulus modality, and congruent and opposite groups of neurons in each module. By incorporating output-dependence in the noise of neural dynamics, we found that the estimates of the integrated posteriors and disparity information agree with Bayesian prediction accurately in the weak input limit. This illustrates the significance of feedback information in neural information processing, and generates an experimentally testable prediction about noisy neural dynamics.

We further show that when the prior has more than one components, additional modules can be used to produce Bayesian prediction of the integrated information. This indicates the close relation between network architecture and the information structure of the environment, as represented by the prior distribution [11]. For the composite prior with a correlated and independent component, the additional module is one that processes direct stimuli. This is readily found in biological systems, which are therefore endowed with the capacity to give Bayesian prediction in complex environment. It is possible to generalize the model to prior distributions with more than two components.

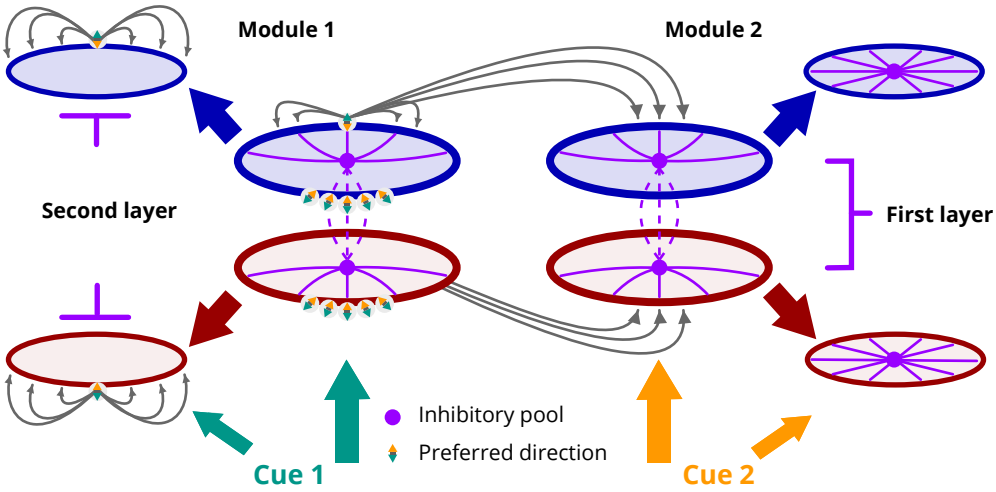


Figure 6.1: Illustration of decentralized model after modification. New modules in the second layer. No connection between two groups of neurons in each module. The inputs and feedforward inputs from the first layer are rescaled by $1 - p_0$ and $p_0$ respectively. Each group of neurons has their own inhibition pool and there's no reciprocal coupling between two modules.

## 6.2 Causal Inference

However, our current model cannot do causal inference. Consider the causal inference structure in [8], the probabilistic model should be rewritten as

$$p(x, s, C) = p(x|s)p(s|C)p(C), \tag{6.1}$$

where $C$ is a hyperparameter for model selection. If we define $C = 0$ and $C = 1$ correspond to segregation and integration models respectively, with assuming the interaction term is a Gaussian, then $p(x, s, C)$ could be approximated by

$$p(x, s, C) \propto \exp[-\frac{(s_1 - x_1)^2}{2\sigma_1^2} - \frac{(s_2 - x_2)^2}{2\sigma_2^2} - C\frac{(s_2 - s_1)^2}{2\sigma_3^2}]. \tag{6.2}$$

In this case, $C$ is similar to $p_0$ which we have been used to rescale the feedforward input strength. That is, this model structure still cannot tell us whether two cues originate from the same source without a known $p_0$. Our future work will focus on extracting $p_0$ from network training for a long-term plan, and further investigation is needed for achieving causal inference in our model.

# References


[1] W.-H. Zhang, H. Wang, A. Chen, Y. Gu, T. S. Lee, K. Y. M. Wong, and S. Wu, "Complementary congruent and opposite neurons achieve concurrent multisensory integration and segregation," *eLife*, vol. 8, p. e43753, 2019.

[2] E. Kandel, J. Schwartz, T. Jessell, S. Siegelbaum, and A. J Hudspeth, *Principles of Neural Science, Fifth Edition*. McGraw-Hill, New York, USA, 2000.

[3] Y. Gu, D. E. Angelaki, and G. C. DeAngelis, "Neural correlates of multisensory cue integration in macaque MSTd," *Nature Neuroscience*, vol. 11, pp. 1201–1210, 2008.

[4] C. C. A. Fung, K. Y. M. Wong, and S. Wu, "A moving bump in a continuous manifold: A comprehensive study of the tracking dynamics of continuous attractor neural networks," *Neural Computation*, vol. 22, no. 3, pp. 752–792, 2010, pMID: 19922292.

[5] W. J. Ma, J. M. Beck, P. E. Latham, and A. Pouget, "Bayesian inference with probabilistic population codes," *Nat Neurosci*, vol. 9, no. 11, pp. 1432–1438, 2006.

[6] C. C. A. Fung, K. Y. M. Wong, and S. Wu, "Dynamics of neural networks with continuous attractors," *EPL (Europhysics Letters)*, vol. 84, no. 1, p. 18002, 2008.

[7] K. V. Mardia and P. E. Jupp, *Directional Statistics*, 01 2000.

[8] K. P. Körding, U. Beierholm, W. J. Ma, S. Quartz, J. B. Tenenbaum, and L. Shams, "Causal inference in multisensory perception," *PLOS ONE*, vol. 2, no. 9, p. e943, 2007.

[9] L. Shams and U. R. Beierholm, "Causal inference in perception," *Trends Cogn Sci*, vol. 14, no. 9, pp. 425–432, 2010.

[10] W.-H. Zhang, H. Wang, K. Y. M. Wong, and S. Wu, "Congruent and opposite neurons: Sisters for multisensory integration and segregation," in *Advances in Neural Information Processing Systems 29*, D. D. Lee, M. Sugiyama, U. V. Luxburg, I. Guyon, and R. Garnett, Eds. Curran Associates, Inc., 2016, pp. 3180–3188.

[11] H. Wang, W.-H. Zhang, K. Y. M. Wong, and S. Wu, "How the prior information shapes neural networks for optimal multisensory integration," *Springer International Publishing*, pp. 128–136, 2017.